Effects of three-body and backflow correlations in the two-dimensional electron gas

Yongkyung Kwon
Department of Physics and Materials Research Laboratory, University of Illinois at Urbana-Champaign, Urbana, Illinois 61801

D. M. Ceperley
Department of Physics and National Center for Supercomputing Applications, University of Illinois at Urbana-Champaign, Urbana, Illinois 61801

Richard M. Martin
Department of Physics and Materials Research Laboratory, University of Illinois at Urbana-Champaign, Urbana, Illinois 61801
(Received 10 February 1993; revised manuscript received 23 June 1993)

We investigate the effects of three-body and backflow correlations on ground-state properties of the two-dimensional electron gas by both variational and fixed-node Green's-function Monte Carlo methods. It is found that the backflow effect is dominant over the three-body effect at high density ($r_s \sim 1$) while they are of equal importance at the lowest density considered ($r_s \sim 20$). With these correlations, we find significant improvements in both variational and fixed-node energies over the Slater-Jastrow results which consider only two-body correlation. The effects are comparable to those in bulk ^{3}He. We present an analytic expression for the correlation energy of the two-dimensional electron gas as a function of the density.

I. INTRODUCTION

The homogeneous electron gas, which is a system of electrons interacting with each other through a $1/r$ potential to which a uniform positive background is added for charge neutrality, is one of the most simple and widely used models to study the electronic motion in two dimensions. This can actually be realized at interfaces of GaAs/$Al_xGa_{1-x}As$ heterostructure and metal-oxide-semiconductor structure[1] and there has recently been a great deal of experimental work[2] on the system. In addition, electrons in two-dimensional (2D) systems are of much interest since the copper-oxide planar structures are crucial to the superconducting properties of high-T_c materials and under strong magnetic fields they display some fascinating phenomena such as the integer and fractional quantum Hall effects. This paper is concerned only with the ground-state properties of the 2D electron gas at zero magnetic field, which have been studied by various approximate methods[3–10] in many-body physics. To calculate the zero-temperature properties of this system, Tanatar and Ceperley[11] used the variational (VMC) and the fixed-node Green's-function Monte Carlo (GFMC) methods with trial wave functions which consisted of the Slater determinant of single-body orbitals and products of two-body correlation functions.

There has been recent progress[12–14] in understanding the importance of higher-order correlations in liquid ^{3}He, a strongly correlated quantum Fermi liquid. When *backflow* effects were put into the Slater determinant, good agreement for the total binding energy with experimental results was obtained.[14] The idea of backflow was originally suggested by Feynman and Cohen[15] based upon conservation of particle current and the variational principle.

In this paper, we consider the effects of *three-body* and *backflow* correlations among electrons. As will be explained in Sec. II, the results of both VMC and fixed-node GFMC method depend upon the trial wave function used. The nodal structure of the wave function is changed by backflow correlations, resulting in lower fixed-node energies. We have investigated how these higher-order correlations affect the ground-state properties, especially correlation energies and pair distribution functions, of the 2D electron gas when compared to the two-body trial function. In our forthcoming paper,[16] we will examine the properties of *particle-hole* excitations with these improved wave functions and try to find the Fermi-liquid parameters of this system. Furthermore, we have found that backflow correlation is crucial to determine the Fermi-liquid parameters because the interactions between quasiparticles with different spins cannot be fully explained without this correlation. Monte Carlo work with backflow correlation was previously done only for bulk ^{3}He.[13,14] To our knowledge, this is the first application to an electron system. We compare our results for the 2D electrons with the previous results for 3D bulk ^{3}He.

All properties of the electron gas without magnetic fields are a function of the dimensionless parameter $r_s = a/a_0$, where a_0 is the Bohr radius, $a = 1/\sqrt{\pi\rho}$ is the radius of a circle which encloses one electron on the average, and ρ is the number density. Using energy units of Ry/electron and length units of a, the Hamiltonian of N electrons is

$$H = -\frac{1}{r_s^2}\sum_{i=1}^{N}\nabla_i^2 + \frac{2}{r_s}\sum_{i<j}^{N}\frac{1}{|\mathbf{r}_i - \mathbf{r}_j|} + \text{const}\,, \quad (1)$$

where the *constant* is the term due to the uniform background of opposite charge. We are here interested in the density range $1 \leq r_s \leq 20$. The ground state of the 2D electron gas at these densities was shown to be in a normal (spin-unpolarized) liquid phase.[11] Most of the experiments on this system have been done for the density range $1 \leq r_s \leq 5$.

In the next section, we introduce the basic scheme of both VMC and fixed-node GFMC methods and show the form of our improved trial wave function including three-body and backflow correlations. In Sec. III, the results of our simulation using both VMC and fixed-node GFMC are presented and we analyze how much these higher-order correlations affect ground-state properties. We also present a new fit to the correlation energy as a function of the density.

II. MONTE CARLO METHOD

In a VMC simulation, one estimates the properties of a given quantum state assuming a trial wave function $\Psi_T(R)$ with the correct symmetry, where R represents a point in the $2N$-dimensional space which describes the positions of N particles. The variational energy is just the average of local energies, $E_L(R) = H\Psi_T(R)/\Psi_T(R)$, if R is sampled with Metropolis algorithm[17] from the probability density function

$$|\,\Psi_T(R)\,|^2 \Big/ \int dR\,|\,\Psi_T(R)\,|^2\,. \quad (2)$$

The choice of a trial wave function is very important in a VMC method like any other variational method. We can get a good upper bound to the exact energy by this method if a reasonable trial wave function is used.

In order to calculate more accurate fermion ground-state properties, the GFMC method is used assuming the fixed-node approximation. In this method, the Schrödinger equation for a many-body system is solved by treating it as a diffusion equation.[18] The Schrödinger equation multiplied by a trial function $\Psi_T(R)$ written in imaginary time t is

$$\frac{\partial f(R,t)}{\partial t} = \frac{1}{r_s^2}\sum_{i=1}^{N}\boldsymbol{\nabla}_i\cdot(\boldsymbol{\nabla}_i f - f\boldsymbol{\nabla}_i \ln\Psi_T^2) - [E_L(R) - E_T]f\,, \quad (3)$$

where $f(R,t) = \Phi(R,t)\Psi_T(R)$ is a probability distribution. The initial ensemble of configurations $\{R\}$ with probability density $f(R,0) = |\,\Psi_T(R)\,|^2$ is evolved forward in time by the above diffusion equation and reaches the equilibrium distribution at sufficiently large t. This equilibrium distribution is determined by the probability density $f(R,\infty) = \Phi(R)\Psi_T(R)$, which is called the *mixed distribution.* Here, $\Phi(R)$ is the lowest-energy eigenfunction of the Hamiltonian which satisfies the fixed-node boundary conditions [i.e., $\Phi(R)\,\Psi_T(R) \geq 0$].[19] The fixed-node approximation is made to avoid the negative weights that would otherwise be generated by the antisymmetric property of fermions. The fixed-node GFMC energy is known to be an upper bound to the exact energy, and usually lies well below the variational energy.[20] We will try to assess how accurate the fixed-node energies are. If the nodes of our trial wave function are the same as those of the exact eigenfunctions, this method gives rise to the exact ground-state properties. This is one of the reasons why a good trial function is very important even in the GFMC method. In addition to that, improved trial functions significantly reduce the equilibration time by initiating the stochastic process nearer the ground state and act to reduce statistical errors.[19]

The usual choice of a trial function is of the Slater-Jastrow type

$$\Psi_T(R) = \det(\varphi_{mn})\,\exp\left(-\sum_{i<j}^{N}u(r_{ij})\right)\,, \quad (4)$$

where $\varphi_{mn} = e^{i\mathbf{k}_m\cdot\mathbf{r}_n}$ for a homogeneous liquid phase and $k_m \leq k_F$ occupied. The nodal structure of the many-body wave function $\Psi_T(R)$ is determined by only the Slater determinant. There are actually two separate determinants for the spin-up and spin-down states because the Hamiltonian of Eq. (1) is spin independent. We use the correlation function $u(r)$ that minimizes the variational energy in the random-phase approximation (RPA) as first derived by Gaskell[21] and determined in Ref. 22 to be nearly optimal. The RPA correlation function for a liquid phase is

$$2\rho\,u_{\rm RPA}(k) = -\frac{1}{S_0(k)} + \left(\frac{1}{S_0^2(k)} + \frac{4v(k)m\rho}{\hbar^2k^2}\right)^{1/2}\,, \quad (5)$$

where ρ is the density of the system, $v(k) = 2\pi e^2/k$ is the Fourier transform of the Coulomb potential, $S_0(k)$ is the static structure factor for the system of noninteracting fermions

$$S_0(k) = \frac{2}{\pi}[\sin^{-1}(y) + y(1-y^2)^{1/2}]\,, \quad (6)$$

and $y = k/2k_F$. This correlation function possesses properties which the optimal one has, such as the cusp condition,[22]

$$\lim_{r\to 0}\frac{du(r)}{dr} = -r_s \quad (7)$$

and the long-range behavior[22] necessary for the correct plasmon dispersion,

$$\lim_{r\to\infty} u\,(r) = 1.48\left[\frac{r_s}{r}\right]^{1/2}\,. \quad (8)$$

With this trial wave function, Ceperley[22] and Tanatar and Ceperley[11] calculated the ground-state properties of the 2D electron gas using both VMC and fixed-node GFMC methods.

In order to get better results for the ground-state properties of this system, we consider improved trial functions which include backflow and three-body correlations and investigate the effects of these correlations. Using the

local energy method in Appendix A, we assume an improved trial wave function which has the form[13,14] of

$$\Psi_T(R) = \det(e^{i\mathbf{k}_i\cdot\mathbf{x}_j}) \times \exp\left(-\sum_{i<j}^{N}\tilde{u}(r_{ij}) - \frac{\lambda_T}{2}\sum_{l=1}^{N}\mathbf{G}(l)\cdot\mathbf{G}(l)\right), \tag{9}$$

where $\mathbf{x}_i$'s are *quasiparticle* coordinates displaced from the real coordinates by a bosonic force

$$\mathbf{x}_i = \mathbf{r}_i + \sum_{j\neq i}^{N}\eta(r_{ij})\,(\mathbf{r}_i - \mathbf{r}_j)\,, \tag{10}$$

$$\mathbf{G}(l) = \sum_{i\neq l}^{N}\xi(r_{li})\,(\mathbf{r}_l - \mathbf{r}_i)\,, \tag{11}$$

and

$$\tilde{u}(r) = u(r) - \lambda_T\,\xi^2(r)\,r^2\,. \tag{12}$$

In addition to the two-body correlation, this improved ansatz includes the three-body correlation $\mathbf{G}(l)\cdot\mathbf{G}(l)$ and the state-dependent correlation $\mathbf{k}\cdot(\mathbf{r}_i - \mathbf{r}_j)\eta(r_{ij})$, which incorporates backflow effects originally introduced by Feynman and Cohen.[15] The latter changes the nodal structure of the wave function. The terms of $-\lambda_T\,\xi^2(r)\,r^2$ cancel two-body terms arising from $\mathbf{G}(l)\cdot\mathbf{G}(l)$. We call $\xi(r)$ the "three-body correlation function" and $\eta(r)$ the "backflow correlation function." We have used spin-independent forms for both three-body and backflow correlations as was done for the two-body correlation.

Our calculations are done for a finite number N of electrons in a square simulation cell with periodic boundary conditions. The Ewald method[11] is used for two-body correlations $u(r)$ to minimize size effects. The correlation functions $\eta(r)$ and $\xi(r)$ are required to go to zero smoothly at a cutoff distance r_c equal to half the side of the simulation cell we use:

$$f(r) \longrightarrow f(r) + f(2r_c - r) - 2f(r_c)\,. \tag{13}$$

The backflow and the three-body correlation function are parametrized as

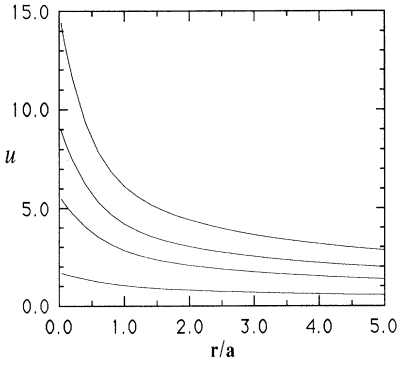

FIG. 1. RPA correlation functions $u(r)$ at $r_s = 1, 5, 10, 20$. The larger r_s values correspond to the larger $u(r)$ at a given r.

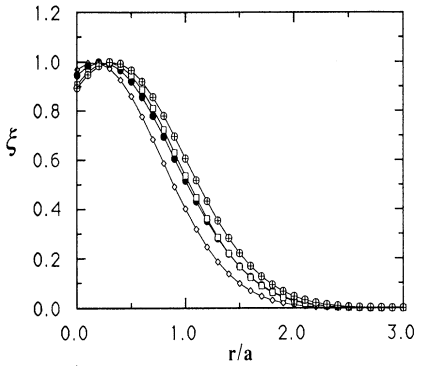

FIG. 2. Optimized three-body correlation functions $\xi(r)$ for $r_s = 1$ (◇), 5 (•), 10 (□), and 20 (⊕).

$$\eta(r) = \lambda_B\frac{1 + s_B r}{r_B + w_B r + r^{7/2}}\,, \tag{14}$$

and

$$\xi(r) = \exp[-(r - r_T)^2/w_T^2]\,. \tag{15}$$

This functional form for $\eta(r)$ satisfies the long-range behavior presented in Appendix A, while our three-body correlation has the same form as that used for liquid ^{3}He in Ref. 14.

In order to optimize our higher-order correlation functions, we minimize the variance of the local energy, defined by

$$V_{\Psi_T} = \frac{\int dR\;\Psi_T^2(R)\,[\,E_L(R) - E_v\,]^2}{\int dR\;\Psi_T^2(R)}\,, \tag{16}$$

using the correlated sampling method.[23,24] If our trial function Ψ_T were the exact ground-state wave function, the variance would be zero. The optimum sets of variational parameters for these correlations, which of course depend upon the density of the system, are given in Table I. Figure 1 shows RPA two-body correlation functions as a function of the density. The forms of optimized backflow and three-body correlation functions are presented

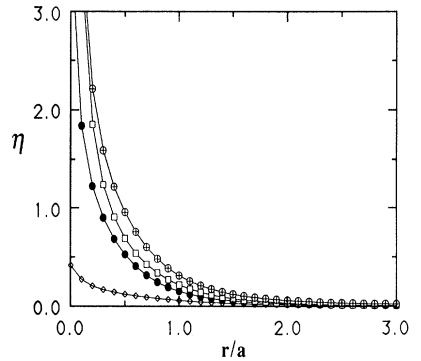

FIG. 3. Optimized backflow correlation functions $\eta(r)$ for $r_s = 1$ (◇), 5 (•), 10 (□), and 20 (⊕).

TABLE I. Optimized variational parameters of *three-body* and *backflow* correlation functions for $N = 58$.

r_s	λ_B	s_B	r_B	w_B	λ_T	r_T	w_T
1.0	0.083	0.761	0.200	1.276	-0.110	0.156	0.883
5.0	0.185	0.299	0.050	0.533	-0.470	0.225	0.954
10.0	0.664	-0.161	0.040	1.516	-0.929	0.284	0.908
20.0	0.262	0.908	0.020	0.582	-0.954	0.322	0.959

in Figs. 2 and 3, respectively, from which it can be seen that our higher-order correlations are short ranged and so the finite-size adaptation in Eq. (13) does not have a significant effect.

The technical difficulty in using a trial function with the backflow correlation is that there is no advantage for moving only one electron at a time because each element of the Slater matrix is a function of all the electronic positions. Therefore, we move all particles simultaneously to increase computational efficiency. The most time-consuming part in this process is to calculate the kinetic energy for a given configuration. An efficient way to calculate these terms is given in Appendix B. The time step (τ_{BF}) in one VMC step with the backflow correlation is about 10% of one (τ_{SJ}) in the Slater-Jastrow simulation. The *efficiency* of VMC,[25] defined by $1/[\mathrm{var}(E_v) \times \mathrm{CPU\ time}]$, with the backflow wave function is about 20% of one with the Slater-Jastrow function (for example, at $r_s = 10$, $\tau_{\mathrm{SJ}} = 23.0$, $\tau_{\mathrm{BF}} = 2.8$, $\mathrm{eff}_{\mathrm{SJ}} = 2.20 \times 10^5$, $\mathrm{eff}_{\mathrm{BF}} = 0.41 \times 10^5$). In GFMC, the Slater-Jastrow trial function is only twice as efficient as the backflow function since the time steps we used are different only by a factor of 2.

III. GROUND-STATE PROPERTIES

A. Monte Carlo results

First we calculated the ground-state properties of the system with $N = 58$ electrons by both VMC and GFMC methods with the Slater-Jastrow trial functions, where the RPA correlation functions of Eq. (5) were used. It can be seen from Table II that our variational energies are equal to those of Tanatar and Ceperley within the error bar at $r_s = 5, 20$ but are different from theirs at $r_s = 1, 10$, while our fixed-node GFMC energies are significantly higher than theirs over the whole density range considered. Their GFMC results are systematically too low. This error approximately cancels the error due to the fixed-node approximation with the Slater-Jastrow function, so that their results are fortuitously close to our present final results.

The same calculations have been done with the improved wave function in Eq. (9). We can see from Table II that both VMC and fixed-node GFMC ground-state energies with the wave functions including backflow and three-body correlations improve significantly the results with the Slater-Jastrow wave functions. Figure 4 shows the effect of backflow and three-body correlations on the remaining correlation energy beyond the Slater-Jastrow variational result and on the correlation energy missing in the Slater-Jastrow fixed-node method. At a high density of $r_s = 1$, the effect by the three-body correlation is negligible and the backflow effect is dominant. However, as the density decreases, the three-body effect increases while the backflow effect decreases. At a low density of $r_s = 20$, the effects of these two correlations are almost the same. We can conclude from the trends of Fig. 4 that at the density where Wigner crystallization occurs, estimated to be $r_s \sim 37$ by Tanatar and Ceperley, the three-body effect will be dominant. This is consistent with the fact that the velocity-dependent backflow correlation is less important as electrons are localized by a strong correlation. The combined effects of both higher-order correlations in the variational wave function account for 60–70 % of the remaining correlation energy beyond the Slater-Jastrow variational energy. At high den-

TABLE II. Variational and fixed-node GFMC energies with various trial wave functions for $N = 58$ in Ry per electron. (TC*, energies obtained by Tanatar and Ceperley with the Slater-Jastrow function in Ref. 11; SJ, the Slater-Jastrow function; 3BD, three-body correlation; BF, backflow correlation.)

Method	Trial wave functions	$r_s = 1.0$	$r_s = 5.0$	$r_s = 10.0$	$r_s = 20.0$
VMC	TC*	-0.3905(3)	-0.2940(3)	-0.16851(5)	-0.09165(4)
	SJ	-0.3879(2)	-0.2936(1)	-0.16837(2)	-0.09164(1)
	SJ+3BD	-0.3894(5)	-0.2947(1)	-0.16895(2)	-0.09195(2)
	SJ+BF	-0.4024(5)	-0.2972(2)	-0.16962(2)	-0.09199(2)
	SJ+3BD+BF	-0.4029(5)	-0.2976(1)	-0.17000(2)	-0.09225(2)
GFMC	TC*	-0.4092(6)	-0.2998(1)	-0.17105(8)	-0.09273(2)
	SJ	-0.4043(5)	-0.2980(1)	-0.17037(2)	-0.09248(1)
	SJ+3BD+BF	-0.4087(2)	-0.2991(1)	-0.17086(1)	-0.09265(1)

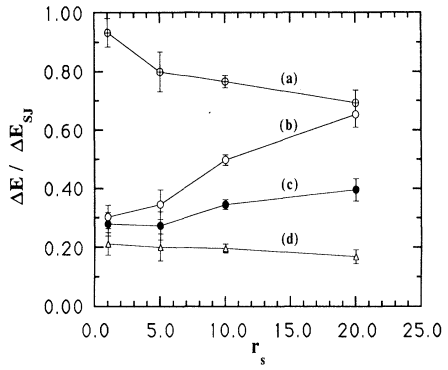

FIG. 4. Effects of three-body and backflow correlations as a function of the density of the system. The vertical axis shows $\Delta E/\Delta E_{\rm SJ} = (E - E^{\rm 3BF}_{\rm GFMC})/(E^{\rm SJ}_V - E^{\rm 3BF}_{\rm GFMC})$, that is, the one corresponds to the Slater-Jastrow variational energy $E^{\rm SJ}_V$ and the zero to the GFMC energy $E^{\rm 3BF}_{\rm GFMC}$ with the trial function including three-body and backflow correlations which is the best estimate of the exact energy available at the present time. (a) shows the effect by the three-body correlation, (b) the effect by the backflow, and (c) represents the combined effect of both correlations. Finally, (d) shows the result by the GFMC method with the Slater-Jastrow function.

sities ($r_s \leq 5$), this variational energy is almost as low as the fixed-node energy from the Slater-Jastrow trial function, which captures about 80% of the remaining correlation energy throughout our density range ($1 \leq r_s \leq 20$) within statistical errors.

Figure 5 shows how the variance of the local energy defined in Eq. (16) changes at $r_s = 10$ depending on the variational energy, that is, the trial wave function. We can see that the variance gets smaller as the variational energy improves. The extrapolation to the zero variance [Fig. 5(c)] gives some idea of the exact energy.

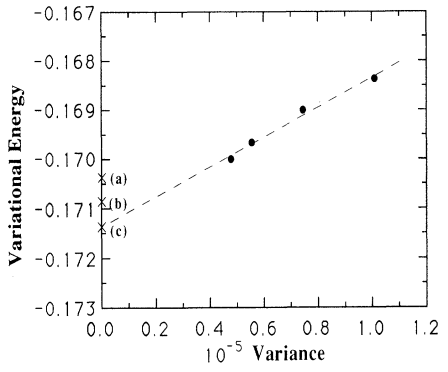

FIG. 5. Variational energy vs variance of local energy with 58 electrons at $r_s = 10$. Each point • represents one variational calculation, (from higher to lower energies) the Slater-Jastrow, three-body, backflow, and (backflow + three-body) results, respectively. Points (a) and (b) show the Slater-Jastrow and the backflow fixed-node GFMC energies, respectively. Point (c) is obtained by the extrapolation through • points. Energy unit is Ry per electron.

We see that this estimate of the exact energy is lower than our best fixed-node result by approximately 0.0005 Ry/electron. Since our extrapolation is quite crude, this must be viewed as a rough estimate of the fixed-node error. Release-node calculations[26] possibly using the maximum-entropy method[27] could be done to get a more accurate estimate of the exact ground-state energy.

The pair distribution function, defined by

$$g(r) = \frac{\pi}{N} \sum_{i \neq j} \langle \delta^2(\mathbf{r}_i - \mathbf{r}_j - \mathbf{r}) \rangle \,, \tag{17}$$

is one of the important microscopic properties of the system which can be calculated by the Monte Carlo methods. First, we calculated these functions by variational methods. Those results could depend upon the trial wave functions used. Figure 6 shows at $r_s = 10$ the Slater-Jastrow variational calculation $g^{\rm SJ}_V(r)$ and how the variational result changes when backflow and three-body correlations are added. It can be seen from Fig. 6(b) that the backflow correlation tends to increase the probability that two electrons are close to each other up to the distance of $1.5a$ while decreasing the probability that two electrons are separated by the mean electron distance ($\sim 2a$), which corresponds to the peak position of the pair distribution function, and beyond that distance. Figure 6(c) shows the three-body correlation makes it more probable that two electrons are very close to each other up to about $0.8a$ and separated by the mean electron distance while making it less probable that the other electrons exist at the distances of $0.8a \sim 1.5a$ [before the peak of $g(r)$] and $2.2a \sim 3a$ (after its peak) from one electron, compared to the Slater-Jastrow result. That is, the backflow correlation makes the shape of $g(r)$ more smooth around its peak and the three-body correlation makes it more structured.

Figure 7 shows the differences at $r_s = 1$, 5, 10, and 20 between two variational pair distribution functions $g^{\rm SJ}_V(r)$, obtained with the Slater-Jastrow trial functions,

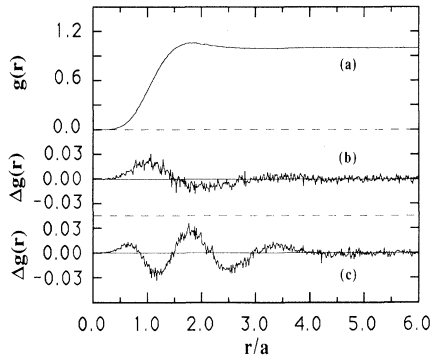

FIG. 6. Variational results for the pair distribution function at $r_s = 10$. (a) shows the Slater-Jastrow result $g^{\rm SJ}_V(r)$, (b) the difference $g^{\rm BF}_V(r) - g^{\rm SJ}_V(r)$ between the Slater-Jastrow result and the result with the trial function including the backflow, and (c) represents the difference $g^{\rm 3BD}_V(r) - g^{\rm SJ}_V(r)$ between the Slater-Jastrow one and the result with the trial function including the three-body correlation.

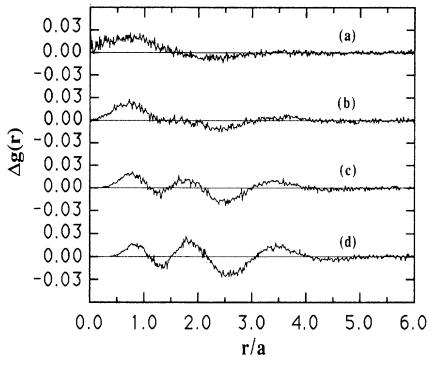

FIG. 7. Differences $g_V^{3BF}(r) - g_V^{SJ}(r)$ between two variational results for the pair distribution function, the Slater-Jastrow result $g_V^{SJ}(r)$, and the result $g_V^{3BF}(r)$ with the trial function including both backflow and three-body correlation at r_s = (a) 1, (b) 5, (c) 10, and (d) 20.

and $g_V^{3BF}(r)$, obtained with the trial functions including both backflow and three-body correlations. The effect of these higher-order correlations at $r_s = 1$ is very similar to that of the backflow correlation alone [see Fig. 6(b)] while the effects at $r_s = 20$ are rather like that by the three-body correlation. These results are consistent with the fact, found by investigating correlation energy differences, that the backflow correlation effect dominates over the three-body correlation effect at a high density regime of $r_s \sim 1$ but the former decreases while the latter increases as the density becomes lower.

The exact pair distribution function $g(r)$ within the fixed-node approximation can be obtained by the GFMC method. The radial pair distribution function $g_M(r)$, calculated with the mixed distribution $f(R,\infty) = \Phi(R)\Psi_T(R)$ in the GFMC method, should be halfway[23] between the variational result $g_V(r)$ and the exact one $g(r)$ if the trial wave function is accurate enough. That is,

$$g(r) \simeq 2g_M(r) - g_V(r) + O[(\Phi - \Psi_T)^2] . \tag{18}$$

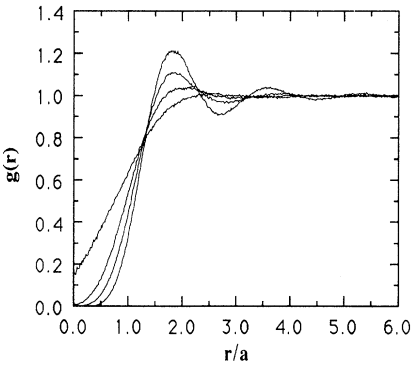

FIG. 8. The extrapolated pair distribution function $g_{ex}^{3BF}(r)$ calculated by the GFMC method with the improved trial function including both backflow and three-body correlation at densities $r_s = 1, 5, 10, 20$. The larger r_s values correspond to more structured forms.

Note that the error in the variational calculation for $g(r)$ is of the first order in $\Phi(R) - \Psi_T(R)$ while the error in this extrapolation process is of second order. Figure 8 shows the extrapolated pair distribution functions $g_{ex}^{3BF}(r)$ calculated by the GFMC method with the trial functions including both three-body and backflow correlations.

B. Analytic expression for correlation energy

Since the present results are the most exact energies known for the 2D electron gas, we have used our results to determine an analytic expression for the correlation energy as a function of r_s. We have followed the same scheme and the same approximations as Tanatar and Ceperley. In order to extrapolate to the thermodynamic limit, the finite-size effects must be assessed. Tanatar and Ceperley employed an extrapolation scheme based upon the Fermi-liquid theory, which assumes that the energy per particle for a finite system is related to the bulk energy by

$$E_N = E_\infty + b_1(r_s)\Delta T_N + b_2(r_s)\frac{1}{N} . \tag{19}$$

Here, ΔT_N is the difference between the kinetic energies of N noninteracting electrons and the infinite system at $r_s = 1$. We determine the parameters E_∞, b_1, and b_2 by a least-squares fit to VMC calculations with Slater-Jastrow trial functions at different values of $N = 26, 42, 58, 74, 114$. In Table III the energies, fitted parameters, and the χ^2 value of the fit are shown. To extract the extrapolated three-body and backflow GFMC energy for the infinite system $E_\infty^{3BF-GFMC}$ it is assumed that the size dependence for the VMC and the GFMC are the same. We did the GFMC runs only at $N = 58$ whose results are shown in Table II and then use the parameters determined from VMC to get $E_\infty^{3BF-GFMC}$.

Having determined the finite-size corrections to the Monte Carlo energies, we now try to obtain the correlation energy of the 2D electron gas in the normal liquid phase as a function of the density parameter r_s. The total energy is the sum of the Hartree-Fock energy E_{HF} and the correlation energy E_c, and the Hartree-Fock energy consists of the kinetic energy and the exchange energy

$$E_{HF} = \frac{1}{r_s^2} - \frac{8\sqrt{2}}{3\pi r_s} . \tag{20}$$

The correlation energies extrapolated to the infinite system at $r_s = 1, 5, 10, 20$ are shown in the bottom row of Table III. In order to fit the energy to a functional form of r_s, we assume the correlation energy can be approximated by

$$E_c = a_0 \frac{1 + a_1 x}{1 + a_1 x + a_2 x^2 + a_3 x^3} , \tag{21}$$

where $x = \sqrt{r_s}$ and the parameters a_i's in this Padé approximant are determined by a nonlinear least-squares fit to the correlation energy at four densities. We use the constraint of $E_c = -0.390 \pm 0.005$ at $r_s = 0$, which was calculated with various methods by several authors.[4–9] The fitted value for each parameter and the resulting χ^2 value are shown in Table IV.

TABLE III. Size dependence in the Slater-Jastrow VMC method of normal electron liquid at $1 \leq r_s \leq 20$ and χ^2-fit parameters. Also shown are the extrapolated GFMC energy at an infinite system ($E_\infty^{\mathrm{3BF-GFMC}}$) and the correlation energy $E_c(r_s)$. The kinetic $\langle T \rangle$ and potential energies $\langle V \rangle$ were obtained by differentiating our fit for the correlation energy (see Sec. III C).

		$r_s = 1.0$	$r_s = 5.0$	$r_s = 10.0$	$r_s = 20.0$
E_V^{SJ}	$N = 26$	-0.3694(4)	-0.2935(1)	-0.16850(2)	-0.09172(1)
	$N = 42$	-0.4429(3)	-0.2960(1)	-0.16899(2)	-0.09179(1)
	$N = 58$	-0.3879(2)	-0.2936(1)	-0.16837(2)	-0.09164(1)
	$N = 74$	-0.4140(3)	-0.2945(1)	-0.16855(2)	-0.09168(1)
	$N = 114$	-0.3967(4)	-0.2937(1)	-0.16833(2)	-0.09161(1)
$E_\infty^{\mathrm{SJ-VMC}}$		-0.3990(4)	-0.2935(1)	-0.16822(2)	-0.09157(1)
$b_1(r_s)$		1.102(7)	0.044(2)	0.0105(5)	0.0023(2)
$b_2(r_s)$		-0.40(2)	-0.046(5)	-0.018(1)	-0.0063(5)
χ^2		2.11	0.13	0.41	0.38
$E_\infty^{\mathrm{3BF-GFMC}}$		-0.4195(6)	-0.2990(2)	-0.17071(4)	-0.09258(2)
$\langle T \rangle$		1.1425	0.0751	0.02519	0.00844
$\langle V \rangle$		-1.5622	-0.3738	-0.19594	-0.10102
$E_c(r_s)$		-0.2191(6)	-0.0989(2)	-0.06067(4)	-0.03506(2)

Figure 9 shows our fitted result for the correlation energy as a function of r_s, along with results obtained by various approximate methods. Compared to the previous Monte Carlo result by Tanatar and Ceperley, our result shows slightly higher correlation energy at $r_s \geq 1$ and lower correlation energy at $r_s < 1$. The fit satisfies the known result at $r_s = 0$ with a χ^2 value being 4.59.

Since our parameters were fit to data only for $r_s \leq 20$, there is no reason to believe our results should describe the correlation energy for $r_s > 20$. Nevertheless, we note that Eq. (21) with our fitted parameters is reasonable even at very low densities because it gives a total energy slightly higher than that for the Wigner crystal as expected. The functional form for the fitted total energy has the asymptotic form

$$E = E_{\mathrm{HF}} + E_c \longrightarrow \frac{\alpha}{r_s} + \frac{\beta}{r_s^{3/2}} + \frac{\gamma}{r_s^2} + \cdots , \qquad r_s \longrightarrow \infty . \tag{22}$$

Our fitted parameters give rise to $\alpha = -2.1448$, $\beta = 0.9928$, and $\gamma = 2.0594$. In the crystal phase, the main contribution to the total energy is a static Madelung term proportional to $-2.2122/r_s$ for the hexagonal lattice which has the lowest Madelung energy in two dimensions.[28] Since we have not studied either the liquid or the crystal at low density, it is not justified to attempt to draw any further conclusions regarding Wigner crystallization from our results. This problem was previously studied by Monte Carlo methods in Ref. 11.

TABLE IV. Parameters of the Padé approximants [Eq. (21)] to the correlation energy determined by a nonlinear least-squares fit and the resulting χ^2 value.

a_0	a_1	a_2	a_3	χ^2
-0.3896	5.5447	2.7861	2.2939	4.59

C. Further analysis

The virial theorem for the electron gas may be written in the form[22,29]

$$2\langle T \rangle + \langle V \rangle = -r_s \frac{dE}{dr_s} , \tag{23}$$

where $\langle T \rangle$ and $\langle V \rangle$ are the kinetic and potential energies per electron. Since $E = \langle T \rangle + \langle V \rangle$, we have

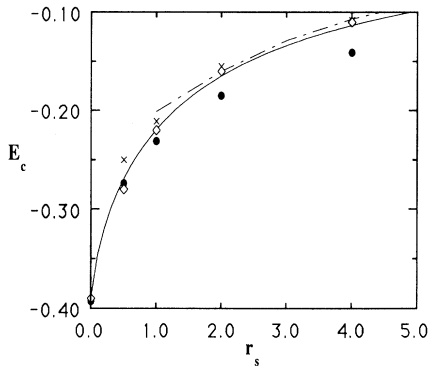

FIG. 9. The correlation energy E_c (units of Ry per electron) as a function of the density parameter r_s. The solid line shows our MC result and the dashed curve is that of Sim, Tao, and Wu (Ref. 10). × represents the STLS calculation of Jonson (Ref. 3). Also shown are the results of Freeman by the coupled-cluster summation in the ring approximation (•, Ref. 5) and in the ladder approximation (◇, Ref. 7).

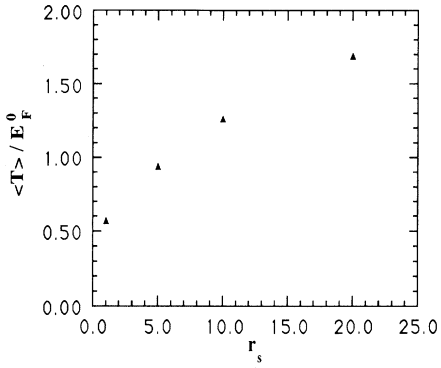

FIG. 10. Kinetic energy $\langle T \rangle$ per electron divided by the Fermi energy E_F^0 ($= 2/r_s^2$ Ry) of the noninteracting system as a function of the density parameter r_s.

$$\langle T \rangle = -\frac{d(r_s E)}{dr_s} , \qquad \langle V \rangle = \frac{d(r_s^2 E)}{r_s dr_s} . \tag{24}$$

Therefore, we can calculate $\langle T \rangle$ and $\langle V \rangle$ from Eq. (24) and our fitted expression for the correlation energy obtained in Sec. III B. The results are shown in Table III.

Figure 10 shows the kinetic energy per electron divided by the Fermi energy ($E_F^0 = 2/r_s^2$ Ry) of the noninteracting system for the densities considered. Correlations always lower the ground-state energy while increasing the kinetic energy above that for the noninteracting system. As expected, the high-momentum tails are more important at small densities, so that $\langle T \rangle / E_F^0$ increases with r_s. The ratio approaches 0.5 as r_s goes to 0.

Figure 11 shows the correlation energies missing from the Slater-Jastrow wave function and from the three-body and backflow wave function divided by the kinetic energy at several densities. Even though we calculated the missing correlation energies for a finite system of $N = 58$, our extrapolation scheme [Eq. (19)] assumes that they have the same values for an infinite system. Less energies are missing at higher densities when compared to the kinetic energies, which reflects a weaker exchange correlation hole. In order to compare our results to another correlated system, we also show in Fig. 11 the same ratios for 3D bulk ^{3}He from Refs. 13 and 14. We see the ratios for ^{3}He are close to the present results for the 2D electron gas.

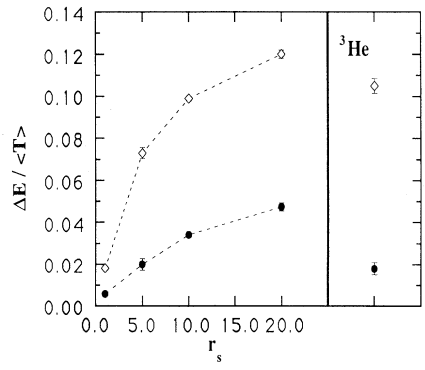

FIG. 11. The energy missing from the Slater-Jastrow wave function (◇) and from the three-body and backflow wave function (•) divided by the kinetic energy as a function of the density parameter r_s. The vertical axis shows $\Delta E/\langle T \rangle = (E_V - E_{\mathrm{GFMC}}^{\mathrm{3BF}})/\langle T \rangle$. The corresponding ratios for bulk ^{3}He were calculated at its equilibrium density (see Refs. 13 and 14).

IV. CONCLUSIONS

We have seen from investigating the correlation energy and the pair distribution function in the ground state of the 2D electron gas that effects of the three-body and the backflow correlation depend upon the density of the system: the backflow effect is dominant over the three-body effect in the high-density regime but the latter is as important as the former at low densities $r_s \approx 20$. The variational wave function including these correlations is a significant improvement over the usual Slater-Jastrow function. Although the energy changes in rydberg units are only 0.015 Ry/electron at $r_s = 1$ and 6.1×10^{-4} Ry/electron at $r_s = 20$, on the scale of interesting phenomena the effects due to these higher-order correlations could be important (note that these changes are 2368 K and 96 K, respectively). At all densities from $r_s = 1$ to $r_s = 20$, we find that three-body and backflow correlations account for approximately 70% of the remaining correlation energy beyond the Slater-Jastrow variational result. Since backflow changes the nodes, we also find that the fixed-node GFMC result is improved significantly. The fixed-node GFMC method based upon the Slater-Jastrow nodes captures only 80% of the remaining correlation energy found with backflow-modified nodes.

We have determined parameters in an analytic expression for the correlation energy as a function of r_s, which fit our calculated energies as well as the known value at $r_s = 0$. The results are given in Eq. (21) and Table IV, and displayed in Fig. 9. Compared to the earlier result of Tanatar and Ceperley, our result shows a significant correction especially at high densities.

Finally, we compare the effects of three-body and backflow correlations in the 2D electron gas with those in bulk ^{3}He. We show the effects are comparable in both systems.

ACKNOWLEDGMENTS

We would like to thank Professor K. E. Schmidt for explaining how to efficiently calculate the second derivatives of the backflow wave function. We also thank V. Rao and G. Ortiz for helpful discussions. This work has been supported by the Department of Energy under Contract No. DEFG 02-91-ER45439 and the National Science Foundation under Grant No. NSF DMR 91-17822. The calculations were performed on the CRAY YMP at the National Center for Supercomputing Applications and IBM RISC/6000 workstations in the College of Engineering at the University of Illinois.

APPENDIX A

In this appendix, we present how we get the form of improved trial functions in Eq. (9) and how the backflow correlation function $\eta(r)$ behaves at a large r. If the trial function $\Psi^{(n)}$ is not orthogonal to the exact ground-state wave function Φ, then

$$\Phi \propto \lim_{t\to\infty} e^{-tH}\,\Psi^{(n)}\,, \tag{A1}$$

where H is the Hamiltonian of the system. Writing this in terms of path integrals using drifting random walks (DRW), we get[19]

$$\Phi \propto \lim_{t\to\infty} \left\langle \exp\left(-\int_0^t E^{(n)}[R(t')]\,dt'\right)\right\rangle_{\rm DRW} \Psi^{(n)}\,, \tag{A2}$$

where $E^{(n)} = H\,\Psi^{(n)}/\Psi^{(n)}$ is a local energy. Up to here Ψ has been a distinguishable-particle wave function. For a fermion system, we antisymmetrize the wave function

$$\Psi_F^{(n)} \propto \sum_P (-1)^P\,P\,\Psi^{(n)}\,, \tag{A3}$$

where P is a permutation operator, $(-1)^P = 1$ for an even permutation and -1 for an odd permutation, and a subscript F means a fermion wave function. We can pull the permutation through the averaging

$$\Phi_F \propto \lim_{t\to\infty} \sum_P (-1)^P\,P \left\langle \exp\left(-\int_0^t E^{(n)}[R(t')]\,dt'\right)\right\rangle_{\rm DRW} \Psi^{(n)}\,. \tag{A4}$$

By letting t be an adjustable variational parameter τ and approximating

$$\left\langle \exp\left(-\int_0^\tau E^{(n)}[R(t')]dt'\right)\right\rangle_{\rm DRW} \simeq e^{-\tau E^{(n)}[R(0)]}\,,$$

we get

$$\Psi_F^{(n+1)}(R) \propto \sum_P (-1)^P\,P\,e^{-\tau\,E^{(n)}(R)}\,\Psi^{(n)}(R)\,. \tag{A5}$$

This is called *local-energy method* to improve a trial wave function.

Suppose we start from a simple Hartree wave function as the zeroth order with plane waves $k \le k_F$ occupied. Equation (A5) will give a first-order wave function of the Slater-Jastrow type. Then the local energy with the Jastrow function has the form of

$$E^{(1)} = \frac{1}{r_s^2}\sum_i \Bigg[\, k_i^2 + 2i\mathbf{k}_i\cdot\boldsymbol{\nabla}_i \sum_{j\neq i} u(r_{ij}) + \nabla_i^2 \sum_{j\neq i} u(r_{ij}) - \left(\boldsymbol{\nabla}_i \sum_{j\neq i} u(r_{ij})\right)^2\Bigg] + V(R)\,, \tag{A6}$$

where $V(R)$ is the Coulomb potential energy. Then the antisymmetrized second-order wave function has the form in Eq. (9), which includes backflow and three-body correlation. Furthermore, we see that $\eta(r)$ and $\xi(r)$ in the improved wave function would be proportional to $\frac{1}{r}\frac{du}{dr}$ at long distance. From the long-range behavior of the two-body correlation $u(r)$ in Eq. (8), the backflow and three-body correlation has the following property:

$$\eta(r), \xi(r) \longrightarrow r^{-5/2}, r \longrightarrow \infty\,. \tag{A7}$$

The approximation going from (A4) to (A5) may cause this long-range behavior for the correlations to be inaccurate. Our choice for the functional form of $\xi(r)$ does not satisfy (A7).

APPENDIX B

We calculate the local energy of a backflow wave function and show that it is $O(N^3)$, where N is the number of particles. We will do it for a general trial function of the form

$$\Psi_T = D\,e^{-u}\,, \tag{B1}$$

where D is the Slater determinant and u involves two- and three-body correlations. Since the local energy is given by

$$E_L(R) = V(R) - \frac{\hbar^2}{2m}\sum_i [\,\nabla_i^2 \ln\Psi_T + (\boldsymbol{\nabla}_i \ln\Psi_T)^2\,]\,, \tag{B2}$$

we need to calculate

$$G_i^\alpha \equiv \nabla_i^\alpha \ln D,\quad K_i \equiv \nabla_i^2 \ln D\,, \tag{B3}$$

where $\alpha = 1, 2$ is x or y and i is the particle index. Let the backflow matrix be $\varphi_{ki} = \varphi_k(\mathbf{x}_i)$, where $\mathbf{x}_i$ is the quasiparticle coordinate and $\varphi_k(\mathbf{x}_i) = e^{i\mathbf{k}_k\cdot\mathbf{x}_i}$ for the electron gas. Then, $D = \det[\varphi_{ki}]$. The following is the procedure for calculating G_i^α and K_i with the numbers in brackets being the computational complexity.

(1) Determine quasiparticle coordinates x_i^α's and their first and second derivatives $[N^2]$:

$$x_i^\alpha = r_i^\alpha + \sum_{j\neq i} \eta(r_{ij})\,(r_i^\alpha - r_j^\alpha),$$
$$A_{ij}^{\alpha\beta} \equiv \nabla_i^\alpha\, x_j^\beta,\quad B_{ij}^\alpha \equiv \nabla_i^2\, x_j^\alpha\,. \tag{B4}$$

(2) Form the backflow matrix and its first and second derivatives $[N^2]$:

$$\varphi_{ki} = \varphi_k(\mathbf{x}_i), \quad \varphi^{\beta}_{ki} \equiv \frac{\partial \varphi_{ki}}{\partial x_i^{\beta}}, \quad \varphi^{\alpha\beta}_{ki} \equiv \frac{\partial^2 \varphi_{ki}}{\partial x_i^{\alpha} \partial x_i^{\beta}} . \tag{B5}$$

(3) Invert the backflow matrix $[N^3]$:

$$\sum_k V_{jk}\, \varphi_{ki} = \delta_{ij}, \quad V_{jk} = \frac{1}{D} \frac{\partial D}{\partial \varphi_{kj}} . \tag{B6}$$

(4) Calculate the intermediate matrix $[N^3]$:

$$F^{\alpha}_{ij} \equiv \sum_k V_{ik}\, \varphi^{\alpha}_{kj} . \tag{B7}$$

(5) Using the chain rule, obtain the first derivatives of the logarithm of the Slater determinant $[N^2]$:

$$G^{\alpha}_i = \nabla^{\alpha}_i \ln D = \sum_{\beta} \sum_j F^{\beta}_{jj}\, A^{\alpha\beta}_{ij} . \tag{B8}$$

(6) Calculate the second derivatives of the logarithm of the Slater determinant $[N^3]$:

$$\begin{aligned} K_i &= \nabla_i^2 \ln D \\ &= \sum_{\alpha,j} B^{\alpha}_{ij}\, F^{\alpha}_{jj} - \sum_{\alpha,\beta,\gamma} \sum_{j,k} A^{\alpha\beta}_{ij}\, A^{\alpha\gamma}_{ik} \\ &\quad \times \left(F^{\beta}_{kj}\, F^{\gamma}_{jk} - \delta_{jk} \sum_m V_{jm}\, \varphi^{\beta\gamma}_{mj} \right) , \end{aligned} \tag{B9}$$

where we have used

$$\frac{1}{D} \frac{\partial^2 D}{\partial \varphi_{kn} \partial \varphi_{jm}} = V_{nk}\, V_{mj} - V_{mk}\, V_{nj} . \tag{B10}$$

[1] T. Ando, A. Fowler, and F. Stern, Rev. Mod. Phys. **54**, 437 (1982).

[2] J. P. Eisenstein, L. N. Pfeiffer, and K. W. West, Phys. Rev. Lett. **68**, 674 (1992); U. Sivan, P. M. Solomon, and H. Shtrikman, *ibid.* **68**, 1196 (1992); I. V. Kukushkin, N. J. Pulsford, K. von Klitzing, K. Ploog, R. J. Haug, S. Koch, and V. B. Timofeev, Phys. Rev. B **45**, 4532 (1992).

[3] M. Jonson, J. Phys. C **9**, 3055 (1976).

[4] A. K. Rajagopal and J. C. Kimball, Phys. Rev. B **15**, 2819 (1977).

[5] D. L. Freeman, Solid State Commun. **26**, 289 (1978).

[6] L. C. Ioriatti, Jr. and A. Isihara, Z. Phys. B **44**, 1 (1981); A. Isihara, Solid State Phys. **42**, 271 (1989).

[7] D. L. Freeman, J. Phys. C **16**, 711 (1983).

[8] S. Nagano, K. S. Singwi, and S. Ohnishi, Phys. Rev. B **29**, 1209 (1984).

[9] Y. Takada, Phys. Rev. B **30**, 3882 (1984).

[10] H. K. Sim, R. Tao, and F. Y. Wu, Phys. Rev. B **34**, 7123 (1986).

[11] B. Tanatar and D. M. Ceperley, Phys. Rev. B **39**, 5005 (1989).

[12] K. E. Schmidt and V. R. Pandharipande, Phys. Rev. B **19**, 2504 (1979).

[13] K. E. Schmidt, M. A. Lee, and M. H. Kalos, Phys. Rev. Lett. **47**, 807 (1981).

[14] R. M. Panoff and J. Carlson, Phys. Rev. Lett. **62**, 1130 (1989).

[15] R. P. Feynman and M. Cohen, Phys. Rev. **102**, 1189 (1956).

[16] Y. Kwon, D. M. Ceperley, and R. M. Martin (unpublished).

[17] N. Metropolis, A. Rosenbluth, M. Rosenbluth, A. H. Teller, and E. Teller, J. Chem. Phys. **21**, 1087 (1953).

[18] P. J. Reynolds, D. M. Ceperley, B. J. Alder, and W. A. Lester, J. Chem. Phys. **77**, 5593 (1982).

[19] D. M. Ceperley, J. Stat. Phys. **63**, 1237 (1991).

[20] D. M. Ceperley and B. J. Alder, Phys. Rev. Lett. **45**, 566 (1980).

[21] T. Gaskell, Proc. Phys. Soc. London **77**, 1182 (1961).

[22] D. Ceperley, Phys. Rev. B **18**, 3126 (1978).

[23] D. M. Ceperley and M. H. Kalos, in *Monte Carlo Methods in Statistical Physics*, edited by K. Binder (Springer-Verlag, Berlin, 1986).

[24] C. J. Umrigar, K. G. Wilson, and J. W. Wilkins, Phys. Rev. Lett. **60**, 1719 (1988).

[25] M. H. Kalos and P. A. Whitlock, *Monte Carlo Methods* (Wiley, New York, 1986), Vol. 1.

[26] D. M. Ceperley and B. J. Alder, J. Chem. Phys. **81**, 5833 (1984).

[27] M. Caffarel and D. M. Ceperley, J. Chem. Phys. **97**, 8415 (1992).

[28] L. Bonsall and A. A. Maradudin, Phys. Rev. B **15**, 1959 (1977).

[29] N. H. March, Phys. Rev. **110**, 604 (1958).